Analytica Chimica Acta 1202 (2022) 339636

Contents lists available at ScienceDirect

Analytica Chimica Acta

journal homepage: www.elsevier.com/locate/aca

Paving the way for examination of coupled redox/solid-liquid interface reactions: 1 ppm Np adsorbed on clay studied by Np M_5-edge HR-XANES spectroscopy

Bianca Schacherl [*], Claudia Joseph , Polina Lavrova , Aaron Beck , Cédric Reitz , Tim Pruessmann , David Fellhauer , Jun-Yeop Lee [1], Kathy Dardenne , Jörg Rothe , Horst Geckeis , Tonya Vitova [*]

Karlsruhe Institute of Technology (KIT), Institute for Nuclear Waste Disposal (INE), P.O. Box 3640, 76021, Karlsruhe, Germany

HIGHLIGHTS

- Paving the way for *in situ* coupled redox/solid-liquid interface reactions analysis.
- Actinide (An) $M_{4,5}$-edge HR-XANES spectroscopy at 1 μg An/g solid achieved.
- Estimated detection limit for speciation studies on mineral surface adsorbed Ans.
- Robust method for exclusion of X-ray beam-induced changes in environmental samples.
- Essential analytical advance for contaminated sites and nuclear waste disposal studies.

GRAPHICAL ABSTRACT

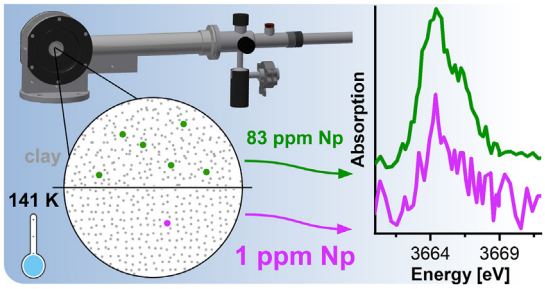

ARTICLE INFO

Article history:
Received 12 December 2021
Received in revised form
6 February 2022
Accepted 17 February 2022
Available online 21 February 2022

Keywords:
Illite
Clay
Detection limit for speciation study
Actinides
Neptunium
High-energy resolution X-ray absorption near-edge structure (HR-XANES) spectroscopy

ABSTRACT

The recently emerged actinide (An) $M_{4,5}$-edge high-energy resolution X-ray absorption near-edge structure (HR-XANES) technique has proven to be very powerful for oxidation state studies of actinides. In this work, for the first time, Np M_5-edge HR-XANES was applied to study Np sorption on illite. By improving the experimental conditions, notably by operation of the spectrometer under He atmosphere, it was possible to measure Np M_5-edge HR-XANES spectra of a sample with ≈ 1 μg Np/g illite (1 ppm). This is 30–2000 times lower than Np loadings on mineral surfaces usually investigated by X-ray absorption spectroscopy. A newly designed cryogenic configuration enabled sample temperatures of 141.2 ± 1.5 K and successfully prevented beam-induced changes of the Np oxidation state. The described approach paves the way for the examination of coupled redox/solid-liquid interface reactions of actinide ions via An $M_{4,5}$-edge HR-XANES spectroscopy at low metal ion concentrations, which are of specific relevance for contaminated sites and nuclear waste disposal studies.

* Corresponding authors.
E-mail addresses: bianca.schacherl@kit.edu (B. Schacherl), tonya.vitova@kit.edu (T. Vitova).
[1] Present address: Pusan National University, School of Mechanical Engineering, 2, Busandaehak-ro 63beon-gil, Geumjeong-gu, Busan, Republic of Korea.

https://doi.org/10.1016/j.aca.2022.339636

1. Introduction

The concept for high-level nuclear waste repositories in deep geological formations consists of a multiple barrier system. Profound understanding of the radionuclide interactions with the installed barriers is crucial in the event of a water-mediated release of radionuclides from the waste containers [1]. The multiple barrier system consists of engineered, geo-engineered and geological barriers. The host rock is part of the geological barrier, and clay rock is one of several candidate host geologies [2–4]. The clay mineral illite is a component of the clay fraction in potential clay host rocks for high-level waste repositories, e.g., the shaly facies of Opalinus Clay [5], Rupelian Boom Clay [6], or Callovo-Oxfordian Clay [7]. The interaction behaviour of long-lived, radiotoxic and redox-sensitive radionuclides of the high-level waste such as ^{237}Np with clay minerals such as illite is intensively investigated in order to understand the type of retention mechanism [8–10].

X-ray absorption near edge structure (XANES) spectroscopy has proved to be a valuable tool for chemical speciation of radionuclides. The spectroscopic technique allows for the identification of oxidation states and provides insight into the electronic structure of the actinide (An) elements [11–15]. The extended X-ray absorption fine structure (EXAFS) technique is used to study the local atomic environment around an absorbing atom. Generally, XANES contains a considerable amount of information, additionally to the oxidation state it is also sensitive to structural changes. However, its interpretation is still often based on fingerprint analyses, which strongly depend on the availability of suitable reference systems. Quantum chemical computations and modelling of spectra could be very successful [16,17], but the use of these methods for geochemical systems is still challenging due to the complexity of the systems. The An $M_{4,5}$-edge high energy-resolution (HR-) XANES technique offers significant advantages [18–23] over the widely applied conventional An L_3-edge XANES spectroscopy [24], in particular: 1) application of an X-ray emission spectrometer improves spectral resolution and 2) the sensitivity to changes in chemical bonding is enhanced by directly probing the An 5f unoccupied states. These aspects cause a significantly improved ability to differentiate between different An oxidation states in mixed redox systems. While there are various examples on the application of U and Pu $M_{4,5}$-edge HR-XANES spectroscopy technique [18–20,22–27], to the best of the authors' knowledge, there are only three studies on Np M_5-edge HR-XANES spectroscopy available in the literature examining Np(VI) in aqueous solution and precipitated Np solid phases [18,21,28]. This method is still unexplored for analysis of diluted Np samples. The present study probes samples, where Np is adsorbed on illite surfaces at trace concentrations and it required significant instrumental development. Such investigations are essential for improving the understanding of mineral surface-induced redox reactions. In general, the examination of the chemical nature of Np sorbed on various surfaces, such as redox state and coordination, is linked with experimental challenges. The following paragraphs discuss relevant issues referring to published Np L_3-edge XANES and EXAFS spectroscopic studies. The literature review highlights the obstacles researchers face by investigating Np sorbed on mineral surfaces using X-ray absorption spectroscopy (XAS). It does not present a comparison between the techniques of EXAFS and XANES, instead the focus of this study is, how the Np M_5-edge HR-XANES technique specifically overcomes the described obstacles by several experimental developments. Those improvements are not explicitly relevant for the EXAFS technique. This is the first report describing Np M_5-edge HR-XANES investigations of surface sorbed Np.

1.1. The detection limit for speciation analysis obstacle

High Np loadings on mineral samples are usually applied to obtain EXAFS spectra with sufficiently high signal-to-noise ratio (S/N). Studies of Np sorbed on iron minerals [29–34], such as hematite or siderite, used by the majority Np loadings > 2000 ppm (Table SI1). For EXAFS studies with Np sorbed on cementitious materials, Np loadings of even > 9000 ppm were reported [35,36]. Sorption mechanisms differ depending on the concentration of sorbing metal ions. Inner-sphere surface complexation of mononuclear An species predominates at relatively low concentrations, while oligomerisation, surface co-precipitation and precipitation of An oxyhydroxides gain relevance at elevated metal ion concentrations [37]. In the case of redox-sensitive elements such as Np, coupled redox and surface sorption reactions take place in environmental systems concomitantly with either (surface) precipitation of Np(IV) oxyhydroxides or sorption of mononuclear Np species depending on the studied concentration ranges [1]. The exact mechanism of surface-induced redox reactions is still a topic of research. However, under the conditions of contaminated sites or in the vicinity of a repository for radioactive waste, Np concentrations will be mostly much lower than traditionally used in XAS studies. Therefore, batch sorption studies with clay rock, specific clay minerals or model minerals reflecting the major surface sites in clay were performed using Np(V) concentrations ranging mostly from 10^{-9} mol/L to 10^{-6} mol/L (cf. Table SI2) [8,9,38,39]. XAS investigations were used in many of these studies to gain knowledge on the chemical nature of surface sorbed Np. However, due to the apparent low sensitivity of XAS, samples with up to four orders of magnitude higher initial Np concentrations than the concentrations used in the respective batch sorption samples were prepared (Table SI2) [9,38,39]. The XAS results obtained at relatively high metal coverages of mineral surfaces obviously cannot be transferred *per se* to the low concentration range (see e.g. Scheinost et al. [31]). This known 'dilemma' is also described by Kalmykov et al. [40], who analysed samples collected from a contaminated aquifer of the Mayak site. In order to allow for the detection of Np via XANES analysis, samples had to be spiked with additional Np. The seeming limitations of XAS sensitivity impairs the applicability of the results to unaltered systems. The complex assessment of the transferability can be eliminated, if an experimental approach is found which allows consistent Np loadings on the mineral surface throughout all experimental methods. In samples, where An phases with comparatively high An content (e.g. AnO_2 nanoparticles) are heterogeneously distributed, μ-XAS, e.g. equipped with a confocal set-up providing high spatial resolution, can be applied to tackle the problem. For instance, Denecke [41] and Terzano et al. [42] reported XANES spectra of 10–60 μm large hot spots of hydrolysed Np(IV) particles despite the very low overall Np content of about 1 ppm. Similar observations were made by Reich et al. [43].

1.2. The beam-induced sample damage obstacle

One way to improve detection sensitivity is to use an X-ray beam with high photon flux [42]. Scheinost et al. [44] discussed that with state-of-the-art beamlines, detection limits of even sub ppm levels are possible. In reality, hitherto reported studies still used relatively high actinide concentrations even though high photon flux synchrotron beamlines were used (e.g. > 10^{12} ph/(s·mm^2) at ROBL, ESRF) [45]. There, Np loadings of about 91–140 ppm (on gibbsite, calcite and Opalinus Clay) could be investigated by EXAFS spectroscopy [46–48]. Heberling et al. [49,50] were able to perform EXAFS analysis of 52 ppm Np sorbed on calcite and Roberts et al. [51] measured XANES of 30 ppm Np co-precipitated with magnetite. However, irradiation of samples with high photon flux very

often bears the risk of beam-induced transitions in the samples, including redox changes, which are frequently not discussed [46–51].

Different types of irradiation effects have been observed for Np-containing samples. Wilk et al. [52] found significant reduction of Np(V) to Np(IV) in their sorption samples of Np on manganese oxide minerals as well as in aqueous solution. In contrast, Denecke et al. [53] observed photo-oxidation of Np(IV) to Np(V) in aqueous solution. It is obvious that effects, often called 'radiation damage' or beam-induced changes, prevent reliable redox speciation notably in water containing samples such as wet environmental samples and wet pastes prepared from batch sorption samples. Those sample changes depend not only on photon flux but also, for instance, on the given sample composition [54–56]. That is why it is important to verify potential beam-induced changes with a Np reference sample in the same physical state and similar matrix [52]. Thorough test measurements are crucial to exclude this obstacle for XAS studies and to ensure the reliability of the data. Additionally, the results of these tests should be comprehensively communicated. The tests can be short repetitive energy scans over the most prominent features of the spectrum, monitoring if the shape is changing with irradiation time. Alternatively, a time-dependent intensity scan at the energy position of the main resonant feature can be conducted to verify if the intensity of this feature is changing [57]. A different way of monitoring beam-induced changes was performed by Arai et al. [34] during the analysis of their data. The authors studied the Np surface speciation on the hematite surface. They found no loss of axial oxygen atoms during their experiment and consequently, excluded beam-induced reduction.

If the beam-induced changes are found to be negligible for a certain time span but prominent after longer X-ray irradiation, the probed region of a sample can be changed after each scan [9]. This approach, however, requires a homogenous species distribution within the sample. Another strategy for suppression of beam-induced changes is to cool the samples below 180 K using a N_2/He cryostat as conducted in the present study [55,56].

The aim of the present study was to obtain speciation information, notably on the redox state of Np adsorbed on the clay mineral illite at low metal ion loadings, using Np M_5-edge HR-XANES spectroscopy while avoiding beam-induced oxidation state changes. To lower the detectable Np loadings, the experimental set-up was optimised; this included the emplacement of the spectrometer within a tight but flexible He flushed casing and applying a liquid N_2 cryostat set-up for cooling the sample during measurements. The experiment was equipped with a multi-sample cell for X-ray emission spectroscopy optimised for both tender and hard X-ray regions including An $M_{4,5}$- and $L_{2,3}$-absorption edges. Technical details can be found in Schacherl et al. [58]. The Np oxidation state was studied in the range from 1 to 209 ppm Np on illite by the advanced Np M_5-edge HR-XANES spectroscopic technique. The effects of beam-induced changes at temperatures of 141.2 ± 1.5 K and 300.0 ± 1.5 K were investigated. This study demonstrates that Np $M_{4,5}$-edge HR-XANES spectroscopy is applicable for samples with Np loadings obtained in batch sorption experiments.

2. Materials and methods

2.1. Illite and Np stock

Samples of Illite du Puy (IdP) [59] containing 6.94 wt.% Fe_2O_3 [60] were purified [61] prior to the batch sorption experiments. The ^{237}Np(V) stock solution, c(Np(V)) = (6.0 ± 0.2) × 10^{-2} mol/L in 0.1 mol/L HCl, was thoroughly characterized [62] and in secular equilibrium with its daughter nuclide ^{233}Pa.

2.2. Np reference samples

Aqueous Np solutions, where Np is present exclusively either in the oxidation state Np(IV) or Np(V) (c(Np) = 0.02 mol/L in 1.5 mol/L HCl), were measured at the Np M_5-edge (further details are available in SI). The Np oxidation state was verified by visible-near infrared (Vis-NIR) spectroscopy before and after the HR-XANES experiments. Np(V) carbonate co-precipitated with uranium carbonate ("Np(V)-cp" = $K_3Na[U,NpO_2(CO_3)_3] \times H_2O$) was used to record Np $M\alpha_1$ fluorescence scans. Its synthesis and characterisation can be found in Vitova et al. [21].

2.3. Solubility calculations

To cover a certain range of Np loadings on illite, samples at pH 5, 7, and 9 were investigated. Speciation calculations with PHREEQC [63] (version 3.4.0; thermodynamic data taken from Guillaumont et al. (2003) [64]) showed that no precipitation of NpO_2(am) or Np(V) solid phase was expected for c_0(Np(V)) = 1 × 10^{-6} mol/L at pH values from 5 to 9 under the redox neutral to slightly reducing conditions present during the batch sorption experiments (redox potential referred to the standard hydrogen electrode amounted to E_h = 280 ± 50 mV). Thus, initial Np(V) concentrations in the batch sorption experiments were selected that solubility limits were not exceeded.

2.4. Batch sorption experiments

A detailed description can be found in SI. Briefly, batch sorption experiments of ^{237}Np on IdP were performed under controlled anaerobic conditions (Ar, 1 ppm O_2 atmosphere) at pH 5, 7 and 9 in triplicate. All suspensions were pre-equilibrated in 0.1 mol/L NaCl at a solid-to-liquid ratio (S/L) of 2 g/L. Initial Np concentrations were selected for series A with c_0(Np(V)) = 1 × 10^{-6} mol/L, for series B with c_0(Np(V)) = 1 × 10^{-7} mol/L and for series C with c_0(Np(V)) = 1 × 10^{-8} mol/L. Np contact times ranged from 11 days (referred to as 'fresh') to 811 days (referred to as 'aged'). To determine the Np loading on IdP, the samples were centrifuged (15 000 rpm = 12 500×g, 80 min) and the amount of Np in the supernatant was determined by inductively coupled plasma–mass spectrometry (ICP–MS). The amount of Np sorbed onto illite was calculated as the difference between the initial Np concentration (Np without illite at pH 1) and the Np remaining in solution (centrifugate). A full sample list can be found in Table 1.

2.5. Np M_5-edge HR-XANES spectroscopy

A glove box encapsulating the X-ray emission spectrometer and the cryostat with the sample holder were developed. A constant He flow enabled a stable oxygen content below 150 ppm during the measurements, which reduced notably the attenuation of tender energy X-ray photons. A Microstat He cryostat (Oxford Instruments, UK) was modified for HR-XANES experiments in the tender X-ray region (2000–5000 eV). A cryostat sample holder was specifically developed to enable very low Np loadings in the HR-XANES experiments. The technical details are described in Schacherl et al. [58]. After centrifugation, the wet Np sorbed illite paste was transferred into the sample holder. It was encapsulated and sealed tightly by two 8 μm Kapton foils under inert gas atmosphere (Ar, 1 ppm O_2 atmosphere). Due to the setup geometry, meaning ≈ 45° between sample and incident beam, this resulted in a total path length of 41 μm through the Kapton foils of the sample holder in the cryostat for the primary and emitted X-ray photons. The sample holder was emerged in liquid N_2 before insertion into the cryostat. Selected samples, detailed in Table 1, were studied with Np M_5-

Table 1
Overview of samples prepared in batch sorption experiments and investigated by HR-XANES spectroscopy (uncertainty of the pH value: ± 0.05), including the noise level (σ_{noise}) and signal-to-noise ratio (S/N) of each averaged sample spectrum.

Sample	c_0(Np(V))/mol/L	pH	Np contact time/d	Np sorbed/ppm	σ_{noise}	S/N
Reference samples						
$Np(IV)_{aq}$	2×10^{-2}	0			3.8×10^{-3}	258
$Np(V)_{aq}$	2×10^{-2}	0			4.1×10^{-3}	246
Np(V)-cp	8.4×10^{-5}					
Sorption samples						
$9A_{fresh}$	1×10^{-6}	9.2	11	83 ± 2	2.4×10^{-2}	42
$9B_{fresh}$	1×10^{-7}	9.2	11	11.9 ± 0.2	6.7×10^{-2}	15
$9C_{fresh}$	1×10^{-8}	9.2	11	1.24 ± 0.04	1.1×10^{-1}	9
$9A_{aged}$	1×10^{-6}[a]	8.4	811	209 ± 4	1.6×10^{-2}	63
$7A_{aged}$ (141 K)	1×10^{-6}[a]	6.9	811	54.6 ± 0.9	4.5×10^{-2}	22
$7A_{aged}$ (300 K)					3.3×10^{-2}	30
$5A_{aged}$	1×10^{-6}	5.2	811	9.8 ± 0.1		

[a] Spiked a second time up to 1×10^{-6} mol/L Np after 11 days of sorption.

edge (3664 eV) HR-XANES spectroscopy at the CAT-ACT beamline for catalysis and actinide science at the KIT Light Source at KIT, Karlsruhe [65]. Further details on the beamline and measurement conditions can be found in the SI.

2.6. Statistical evaluation

The spectra were normalised to [0,1] by setting the maximal signal to unity after subtracting the data point with the lowest signal from each data point of a given spectrum. Subsequently, the noise level, σ_{noise}, was determined as the standard deviation (σ) of the absorption signal in the energy pre-edge region (3658 eV−3661.5 eV) of the respective sample spectrum according to Eq. (1). Note, no absorption features are present in this spectral region, thus all derivations of the signal from a constant offset is attributed to noise. A_E is the absorption signal at a defined incident energy E, $\overline{A}$ is the average signal and n is the number of data points.

$$\sigma_{noise}(\text{sample}) = \sigma[A(3658\ \text{eV}-3661.5\ \text{eV})] = \sqrt{\frac{\sum_{E=3658\ eV}^{E=3661.5\ eV}(A_E-\overline{A})^2}{(n-1)}} \quad (1)$$

For each sample spectrum, the respective absorption intensity at the energy position of the white line (WL) maximum was divided by the respective σ_{noise} value to determine S/N (see Table 1). This methodology lowered the importance of sample and measurement parameters and increased the comparability of spectra obtained at different beamlines or for different sample systems using the respective S/N. To compare two spectra, the incident energies were rebinned on an energy grid with a step size of 0.2 eV. Two spectra were identified as statistically significant different, when the difference obtained by subtracting the normalised absorption signals from each other, Δ, exceeds ± 2σ (cf. Fig. 1B). The 2σ confidence interval for the difference of two independent spectra was calculated using the error propagation law (Eq. (2)):

$$2\sigma(\Delta_{1,2}) = \sqrt{(2\sigma(\text{spectrum sample 1}))^2 + (2\sigma(\text{spectrum sample 2}))^2} \quad (2)$$

The impact of possible beam-induced changes often called 'radiation damage' was examined by comparing spectra of a sample exposed for different time periods to synchrotron radiation. In order to identify possible changes, the 2σ variation of individual data points of a spectrum averaged from 9 individual spectra was examined.

3. Results and discussion

3.1. Spectral features of $Np(V)_{aq}$ and $Np(IV)_{aq}$ and sorbed Np species

Np(V) in an acidic to pH-neutral aqueous solution forms covalent, *trans*-dioxo bonds (NpO_2^+, neptunyl) with five water molecules weakly bound in the equatorial plane [66,67]. Np(IV) in strongly acidic aqueous solution is bound to approximately ten water molecules [66–68]. The Np M_5-edge HR-XANES spectrum of $Np(V)_{aq}$ shows a strong absorption peak at 3664.1 eV (*A*), also called white line (WL), and a distinct shoulder feature at 3667.15 eV (*B*) (Fig. 1A). The spectrum of $Np(IV)_{aq}$ exhibits a relatively broad and intensive WL with its maximum trending to slightly higher energies compared to $Np(V)_{aq}$ (*A*). The peak shows a sharp decrease in intensity in the higher energy region with no clear second peak. Usually, a higher energy position of peak *A* would be expected for a higher metal oxidation state. The shift to a lower energy for the higher Np oxidation state can be explained with the covalency of the *trans*-dioxo bond. It leads to charge transfer from the oxygen atoms to Np(V) resulting in a higher electron density on Np and increasing screening of the nuclear charge of $Np(V)_{aq}$ compared to $Np(IV)_{aq}$. Similar effects can be observed in Np L_3-edge XANES spectra, where also a higher energy position for the absorption edge would be expected for higher oxidation states. Instead, the absorption edge of $Np(V)_{aq}$ is at the same position as the absorption edge of $Np(IV)_{aq}$ [12,68,69]. Feature *B* can be assigned to electronic transitions of 3d electrons to the unoccupied σ-antibonding orbital of NpO_2^+ as identified for neptunyl, as well as uranyl and plutonyl solid and liquid phases in Vitova et al. [18,21,70–72]. Therefore, this feature with strong intensity can be used to detect neptunyl species. The large ligand field splitting of the 5f unoccupied orbitals leads to the well resolved peak *B* in the An $M_{4,5}$-edge HR-XANES spectra, which is characteristic for the actinyl series.

According to geochemical calculations, neither Np(IV) nor Np(V) precipitates should form under the chosen experimental conditions. Consequently, spectra for Np-illite samples represent exclusively Np species sorbed on illite surfaces. The spectrum of sample $9A_{fresh}$ (83 ± 2 ppm Np, Fig. 1A) shows a distinct shoulder (*B'*). This shoulder feature shows an energy shift towards lower energies compared to feature *B* in the $Np(V)_{aq}$ spectrum. The energy splitting between features *A* and *B'* is approximately 0.85 eV smaller than between features *A* and *B* in $Np(V)_{aq}$. This trend is also well visible in the difference plot $\Delta(9A_{fresh,}\ Np(V)_{aq})$=$9A_{fresh}$-$Np(V)_{aq}$ (red spectrum) and $\Delta(9A_{fresh,}\ Np(IV)_{aq})$ (green spectrum) with a confidence interval of ± 2σ, respectively, marked in Fig. 1B. The horizontal orange straight line represents $\Delta(9A_{fresh},\ 9A_{fresh})$. At the approximate energy position of shoulder *B'* (vertical orange dashed

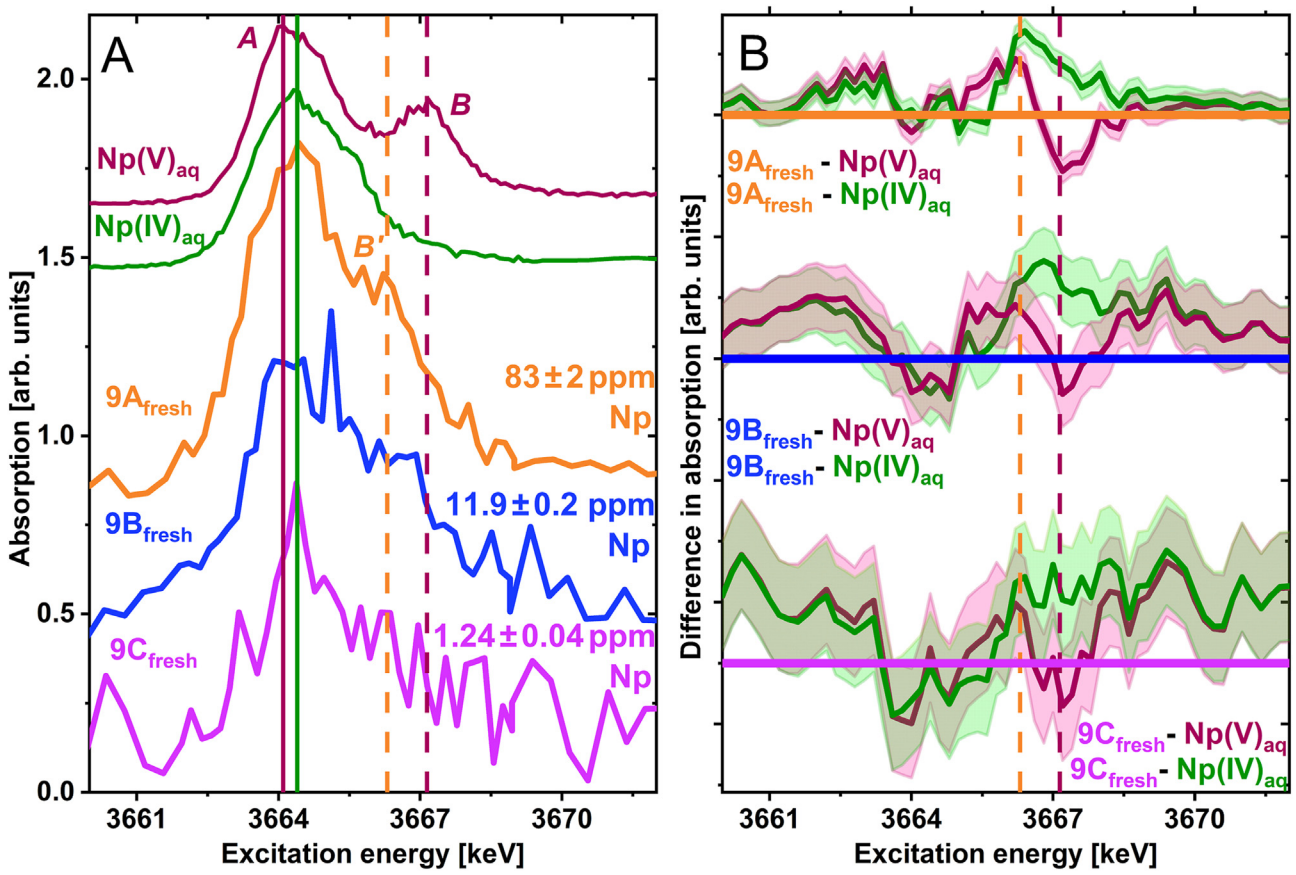

Fig. 1. A) Np M_5-edge HR-XANES spectra of the aqueous references $Np(V)_{aq}$ and $Np(IV)_{aq}$ and the sorption samples $9A_{fresh}$ (83 ± 2 ppm), $9B_{fresh}$ (11.9 ± 0.2 ppm) and $9C_{fresh}$ (1.24 ± 0.04 ppm). The features A, B and B′ are indicated. All spectra of Np-illite samples were recorded at 141.2 ± 1.5 K. B) Difference plots of the sample spectra in A), the shaded green and red areas correspond to a confidence interval of ± 2σ. (Please refer to the online version for a coloured figure.)

line), the difference plot $\Delta(9A_{fresh,}\ Np(V)_{aq})$ shows a maximum while a minimum occurs at the energy position for feature *B* (vertical dark red dashed line). This finding illustrates that the spectrum of $9A_{fresh}$ contains additional speciation information beyond the Np oxidation state. In detail, it indicates the decrease of the Np(V)-O_{ax} bond covalency for sorbed Np [18] and reflects differences in the Np(V) bonding environment at the illite surface as compared to Np(V) in aqueous solution. Qualitatively, the relatively narrow WL feature shows that Np(V) was the predominant oxidation state in this sample. The interpretation of the slight trend to higher energies of feature *A* for Np-illite samples as compared to $Np(V)_{aq}$ still needs to be discussed (cf. vertical green line in Fig. 1 as compared to the dark red line marking the WL position of the $Np(IV)_{aq}$ and $Np(V)_{aq}$ spectrum, respectively). This shift might be a consequence of Np(V) coordination to clay surface hydroxyl groups. However, the WL maximum lies close to that of the $Np(IV)_{aq}$ spectrum. Partial reduction of Np(V) on the illite surface as proposed by Marsac et al. [9] may, therefore, also explain the observed energy shift. This observation highlights the need for further X-ray spectroscopic studies on Np surface complexes. For quantitative speciation analysis, for instance using linear combination least squares fit analyses, precise and comprehensive analyses of appropriate reference systems needs to be performed [13,21]. This will be subject to future studies.

3.2. Detection limit estimate for speciation studies of Np sorbed on illite

Major components of air such as O_2 and N_2 absorb and strongly scatter X-rays with energies in the tender X-ray region (2000–5000 eV). Consequently, X-ray spectra at these energies are best recorded in the absence of air. Furthermore, traces of Ar in sample containments should be ideally avoided, since the Ar K-edge absorption energy is at 3206 eV, i.e. near the $M\alpha_1$ fluorescence energy of Np (3261 eV). The presence of Ar would result in a drastic reduction of intensity of both the incident X-ray beam and the emitted Np $M\alpha_1$ fluorescence. The investigation of samples with very low Np loading (1–80 ppm) was only possible in the present study by major improvements of the equipment, i.e. (1) a tight glove box filled with He enclosing the X-ray emission spectrometer; (2) the investigation of cooled samples by including a cryostat for tender X-ray energies in the experimental setup; and (3) a sample holder equipped with three thin Kapton windows (12.5 μm and 2 × 8 μm) with a new tightening concept. The experimental set-up is described in detail in Schacherl et al. [58].

To determine the Np loading, which was still detectable by the improved setup, highest comparability of the Np-illite spectra was necessary. This was achieved by the application of similar sorption conditions (pH 9, S/L = 2 g illite/L, 0.1 mol/L NaCl, sorption time = 11 days). Only the initial Np concentration was stepwise reduced by an order of magnitude each from sample $9A_{fresh}$ over sample $9B_{fresh}$ to sample $9C_{fresh}$. Consequently, this resulted in a stepwise decrease of Np loadings on illite. The spectra from the three samples are depicted in Fig. 1A. Alongside feature *A*, the *B*′ feature is clearly visible in the spectra and the difference plots, this indicates the predominance of Np(V) in both $9A_{fresh}$ (83 ± 2 ppm Np) and $9B_{fresh}$ (11.9 ± 0.2 ppm Np) samples (cf. Fig. 1B). The shift of feature *B*′ to lower energies indicates a different Np speciation in

$9A_{fresh}$ and $9B_{fresh}$ than in $Np(V)_{aq}$. The features of the spectrum are less pronounced in $9B_{fresh}$, where the Np content is lower. By averaging two scans measured 10 h each, it was possible to record the spectrum of the $9C_{fresh}$ sample containing 1.24 ± 0.04 ppm Np (Fig. 1A). The spectral shape is similar to $9A_{fresh}$ and $9B_{fresh}$. The spectrum of $9C_{fresh}$ exhibits a relatively narrow WL feature and a shoulder region, too. As expected, a significant σ_{noise} is present. The S/N was quantified with 9, much lower than the S/N of $9A_{fresh}$ (42) and $9B_{fresh}$ (15) (Table 1). The larger influence of noise is also visible in the larger ± 2σ confidence interval area in the difference plots. The detection limit criteria for any element or edge is S/N > 3. As a conclusion, the WL signal for Np at the M_5-edge of $9C_{fresh}$ with S/N equal to 9 and a Np loading of about 1 ppm is considered above the detection limit. However, based on the observable features and under consideration of the ± 2σ confidence interval in the respective difference plots, 1 ppm lies on the verge or shortly below the limit of Np loading, where an oxidation state or speciation study of Np sorbed on illite at the CAT-ACT beamline with the current set-up is possible. Nevertheless, it can be stated, that in comparison to previous studies [9,29–36,38,39,46–52], the spectra in the present study are obtained for samples with a factor of 30–2000 lower Np loading.

3.3. Elimination of beam-induced changes of Np oxidation state

Previously, the $Np(IV)_{aq}$ and $Np(V)_{aq}$ spectra were measured at the Np M_5-edge for samples with high Np concentrations ($c(Np) = 2 \times 10^{-2}$ mol/L) at room temperature. These measurements were recorded with a previous He-box configuration, in a He atmosphere with higher air content. Chemical changes of the Np samples induced by irradiation were tested by recording quick HR-XANES scans (1 min/scan). Within this illumination time, no changes of the spectra indicating X-ray induced oxidation state variations of Np were found. This could be explained by the reduced intensity of the incident X-ray beam as a result of the high air content in the box encapsulating the spectrometer. Complementary, beam-induced changes in liquid samples were checked with Vis-NIR spectroscopy. The energy positions and intensities of the features in the Vis–NIR spectra are very sensitive towards changes of the Np oxidation state. The Vis-NIR measurements were performed for $Np(IV)_{aq}$ and $Np(V)_{aq}$ before and after HR-XANES experiments (Fig. 2). Both sets of spectra show similar features, which is an additional strong indication, that beam-induced changes were avoided for these highly concentrated Np samples.

In order to successfully measure Np oxidation states in the low ppm range of Np, it was mandatory to reduce the amount of air in the box enclosing the X-ray emission spectrometer. As a result of this improvement, the emitted fluorescence photons were less attenuated. However, the intensity of the incident photon flux also increased. Consequently, beam-induced changes of the Np oxidation state became visible in sorption samples measured at room temperature already after a few minutes of X-ray irradiation. The Np M_5-edge HR-XANES spectrum of sample $7A_{aged}$ recorded at 300.0 ± 1.5 K is shown in Fig. 3. The spectrum exhibits a relatively broad feature *A* and almost no shoulder *B′*, thus it resembles the spectrum of $Np(IV)_{aq}$. The disappearance of feature *B′*, typical for Np(V), after extended irradiation time is strongly suggesting the reduction of Np(V) to Np(IV). The beam-induced oxidation state change of Np can be minimised by cooling the sample as demonstrated for sample $7A_{aged}$ in Fig. 3. A narrow feature *A* and a shoulder feature *B'* are visible in the spectrum of the $7A_{aged}$ sample measured at 141.2 ± 1.5 K. The difference between the spectra of the sample $7A_{aged}$ measured at 141.2 ± 1.5 K and at RT is statistically significant as visualised by the peak in the difference plot in Fig. 3 (cf. vertical dashed orange line). This finding demonstrates that sample $7A_{aged}$ measured at 300 K showed beam-induced changes of Np, which most likely caused reduction to Np(IV).

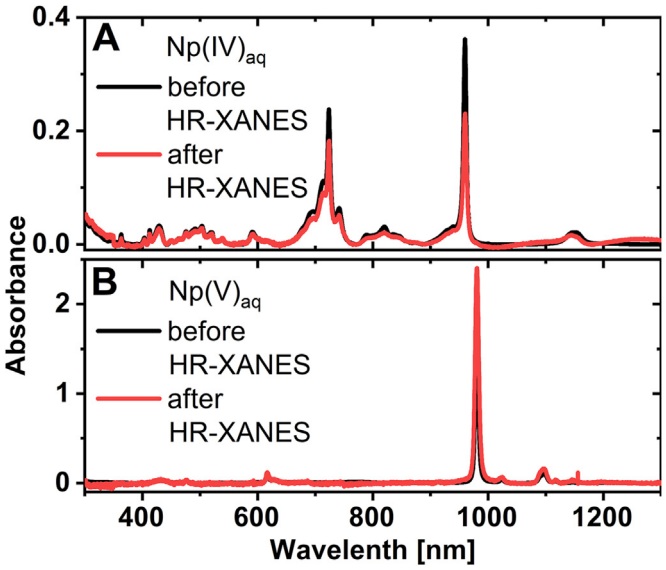

Fig. 2. Visible near-infrared spectra of A) $Np(IV)_{aq}$ and B) $Np(V)_{aq}$ samples measured before and after HR-XANES spectroscopy (sample volume: 200 μL, cuvette path length: 2 mm).

At the CAT-ACT beamline, the flux density was determined to be

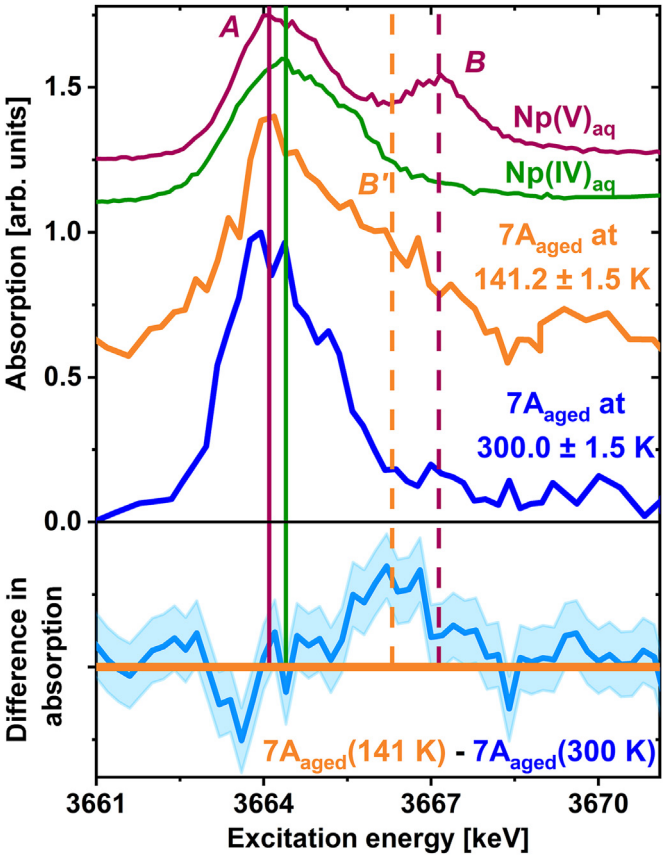

Fig. 3. Np M_5-edge HR-XANES spectra of the aqueous references $Np(V)_{aq}$ and $Np(IV)_{aq}$, and sample $7A_{aged}$ at 141.2 ± 1.5K (54.6 ± 0.9 ppm) and at 300.0 ± 1.5 K. Below: Difference plot for Δ($7A_{aged}$ (141 K),$7A_{aged}$ (300 K)), the shaded blue area corresponds to a confidence interval of ± 2σ. (Please refer to the online version for a coloured figure.)

$(5.2 \pm 0.2) \times 10^{10}$ ph/(s·mm^2) at 3664 eV incident energy. At 300 K, Wilk et al. [52] found 78 ± 12% of Np(IV) in a NpO_2^+ control solution after X-ray irradiation. The X-ray irradiation time per sample is unknown for Wilk et al. [52], but the flux density could be estimated from the beamline characteristics [73] and amounted to about 5×10^{10} ph/(s·mm^2). This value is comparable with the photon flux in the experiments described in the present study. The present observations are also consistent with the studies of Göttlicher et al. [55] and Steininger et al. [56]. They found that Cr(VI) sorbed onto kaolinite was reduced by X-ray radiation to lower Cr oxidation states, since the Cr(VI) signal decreased, during irradiation at 270 K with a photon flux of 1.5×10^{11} ph/(s·mm^2). But at temperatures below 180 K, beam-induced changes could be prevented. The authors found, that for photon flux densities higher than 10^{12} ph/(s·mm^2), beam-induced changes of sorbed Cr(VI) were inevitable over time even at a temperature of 15 K. These findings are important to consider when investigating similar samples at high photon flux beamlines.

The occurrence and extent of beam-induced changes of samples depend on many factors, not only on the photon flux as shown by Van Schooneveld and DeBeer [54]. In an extensive study, they showed that there is no exclusive dose-photoreduction correlation for Fe and Mn L-edge (640–720 eV) investigations of model systems such as $K_3[Fe(CN)_6]$ and $KMnO_4$. The authors discussed the irradiation effects on different oxidation states and absorption edges of Fe and Mn as well as the combination of factors like temperature, pressure and sample conditions. Also, Göttlicher et al. [55] and Steininger et al. [56] highlighted the importance of the sample matrix, for instance, cellulose being more susceptible to beam-induced changes than boronitride. On the basis of these results, the selection of a representative reference system, where beam-induced changes can be monitored, has high importance. In the present study, $9A_{aged}$ (209 ± 4 ppm Np) was chosen for beam-induced damage tests at 141.2 ± 1.5 K. The matrix and measurement geometry of this sample was consistent with all other sorption samples analysed in this study. Repetitive measurements on the same sample spot showed no substantial changes or trends in the spectra within the 2σ confidence interval calculated for each point considering 9 single spectra (Fig. 4). This demonstrated that no beam-induced changes were caused in this sample.

A total irradiation time of 240 min was covered with these tests. For very dilute samples, where even longer scan times were needed, the total scan time was divided in at least two equally long scans. The raw data of these scans were thoroughly compared for any changed features in the spectra before averaging. As a result, beam-induced changes could be ruled out in this system at 141.2 ± 1.5 K for up to 20 h total irradiation time. The σ_{noise} in the single spectra were, in accordance with the central limit theorem, larger than the σ_{noise} of the final averaged spectrum. These averaged spectra with their individual σ_{noise} are compared in this study (Fig. 1, Fig. 3, Fig. 4 black trace), they should and were not compared to single scan spectra.

3.4. Potential for further optimisation

The presented results using the current set-up display a significant improvement for the An $M_{4,5}$-edge HR-XANES spectroscopy on dilute samples. But there is still potential for an increase of S/N, which can lead to reliable oxidation state analyses for 1 ppm Np or even lower Np loadings. For instance, the interference of the X-rays elastically scattered from the sample and the characteristic fluorescence emitted from other elements present in the clay can be minimised in the detected signal. How both effects are influencing the Np XANES spectrum shall be discussed briefly. Illite du Puy contains significant amounts of potassium (7.82 wt.% K_2O [60]). The

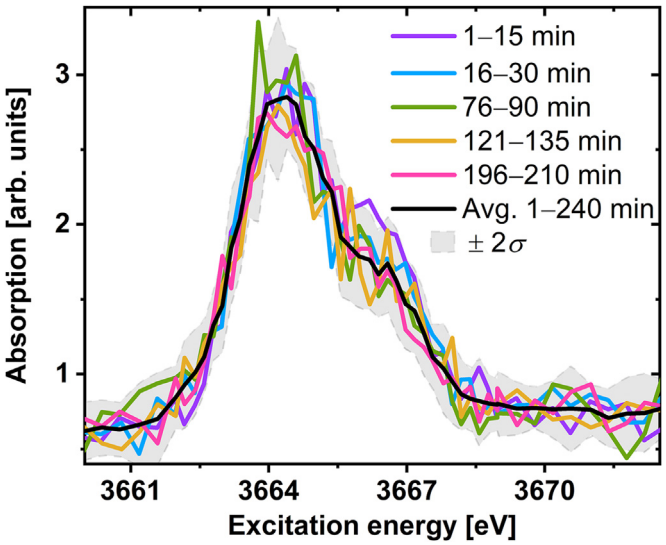

Fig. 4. Test for beam-induced changes of Np oxidation state in sample $9A_{aged}$ (209 ± 4 ppm) (single scans) as a function of X-ray irradiation duration at 141.2 ± 1.5 K. The average of all single scans is shown in black with the corresponding ± 2σ confidence interval calculated for each individual data point (grey area).

K K-edge absorption energy is at 3607.4 eV. Fig. 5A depicts the K $K\alpha_{1,2}$ characteristic fluorescence lines of sample $5A_{aged}$. These lines have 50 eV energy difference compared to the Np $M\alpha_1$ fluorescence emission and can be very well separated by the X-ray emission spectrometer (energy resolution, $\Delta E \approx 1$ eV [18], cf. Fig. 5A). However, a small fraction of the K Kα-fluorescence, in every measurement, directly reaches the detector (green arrow in the inset of Fig. 5B). Unfortunately, the Np Mα and K Kα fluorescence signals cannot be resolved by a solid-state detector ($\Delta E > 100$ eV) used in the present study. For samples with high analyte loadings, this unwanted, interfering signal is negligibly small, but for low analyte loadings, it can have a considerable effect. This is visible in Fig. 5B, where the fluorescence spectrum of sample $9A_{fresh}$ is depicted measured by the detector for excitation energies (E_{inc}) well above (red spectrum) or below (green spectrum) the Np M_5 absorption edge. The elastically scattered incident beam contributes, too (blue arrows in the inset of Fig. 5B). These effects are particularly significant for low loading samples with relatively high fractions of interfering elements (e.g. K in the case of Np). Then, the intensity of the direct emission from the interfering element is significant compared to the emission intensity from the element of interest. One solution for minimising contributions of elastic scattering and fluorescence signals from other elements than Np would be to mount a slit with defined width in front of the detector. Besides the detector modification, the sample holder geometry can be improved. So far, the irradiated sample areas were only marginally larger than the beam size, which led to signal loss due to minor beam instability. This can be overcome with sample holders with larger sample areas.

An additional possibility for improvement of the S/N of Np M_5-edge HR-XANES spectra lies in the measurement parameters. As it is performed in the present study, the XANES spectra are usually recorded by positioning the analyser crystals at the maximum intensity of the normal emission line. This is identified as the maximum of the emission intensity at incident energies above the absorption edge ($E_{inc} = 3700$ eV). However, higher intensity is often observed at the absorption edge itself at a different emission energy (known as the resonant emission energy). If the resonant emission energy is used to record the Np M_5-edge HR-XANES spectra, it can

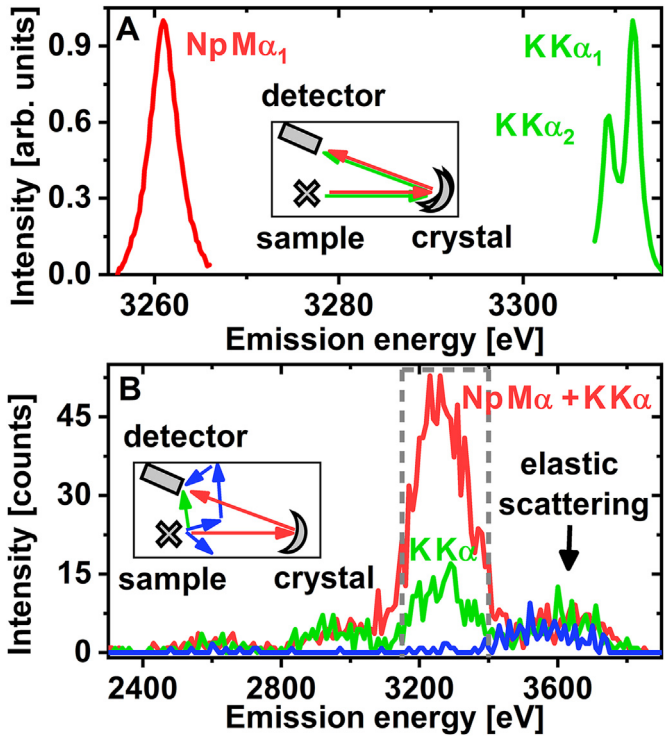

Fig. 5. A) Np $M\alpha_1$ of sample Np(V)-cp (red) and K Kα of sample $5A_{aged}$ (green); B) The solid-state detector signal collected for 90 s using excitation energy above (red, $E_{inc} = 3664$ eV) or below (green, $E_{inc} = 3654$ eV) the Np M_5-edge and below the K K-edge (blue, $E_{inc} = 3590$ eV). The spectra are recorded of sample $9A_{fresh}$ (red and green) and of the Al_2O_3 sample holder (blue). The insets depict the set-up and origin of the predominant signals for samples with high Np/K loadings (A) and low Np loadings (B). The region of interest (ROI) integrated to obtain the spectra is marked with grey dashed lines. (Please refer to the online version for a coloured figure.)

improve the count rate by approximately 30% (exemplary for sample Np-cp) [21]. Before this can be applied for samples with low Np loading, the energy positions of the intensity maxima of the resonant emission for the different Np oxidation states have to be better understood and a procedure for measurement of references has to be developed.

As a last point, analyser crystals with 0.5 m bending radius, as opposed to 1 m in the current study, can be applied. This would increase the photon collection efficiency. Since the Bragg angle using the Si(220) reflection of the crystals is large (81.9°) and therefore favourable for recording Np M_5—edge HR-XANES spectra, no substantial loss of spectral energy resolution is expected.

4. Conclusion

For the first time, Np M_5-edge HR-XANES spectroscopy on Np sorbed on illite was performed. Notably, M_5-edge HR-XANES spectra for this system were recorded down to 1.24 ± 0.04 ppm of Np. Apparently, the chemical environment of adsorbed Np has a significant impact on the spectral shape. Therefore, the unequivocal discrimination of Np redox states requires further investigations using appropriate reference samples. Detailed study and elimination of beam-induced changes of the Np on clay samples is mandatory as illustrated in this study. It was shown that such beam-induced Np oxidation state changes for the present photon flux densities ($(5.2 \pm 0.2) \times 10^{10}$ ph/(s·mm^2) at 3664 eV) at the CATACT beamline could be excluded by cooling the samples down to 141.2 ± 1.5 K. With further experimental optimisation, a higher S/N and thus Np speciation at 1 ppm or even lower Np loadings should be achievable. These findings demonstrate that it is possible to perform in parallel HR-XANES and batch sorption experiments over a range of Np concentrations down to trace level. Note, based on the instrumental improvements, the detection limit achieved is valid for Np M_5-edge HR-XANES spectroscopy. It is expected to be similar for all An $M_{4,5}$ and most $M_{1\text{-}3}$ absorption edges from U to Cm. High diffraction order for the used analyser crystals and an as close as possible to 90° Bragg angle are required for low detection limits. In the case of EXAFS spectroscopy, one of the described technical improvements, i.e. cooling down the sample to cryogenic temperatures, will reduce beam-induced oxidation state changes. However, different experimental improvements are required to achieve lower detection limits for EXAFS spectroscopy, which will be the focus of future work. The described technique provides Np speciation information for a large range of analyte concentrations, which allows for a consistent understanding and modelling of molecular scale spectroscopic data and macroscopic batch sorption data. Spectroscopic methods optimised towards highest sensitivity will allow as well for the direct examination of An oxidation states at low loadings, which are very often observed in contaminated sites and which are typical for the expected An behaviour in repository systems.

Funding sources

This project has received funding from the European Union's Horizon 2020 research and innovation program under grant agreement No. 847593.

Author information

The manuscript was written through contributions of all authors. All authors have given approval to the final version of the manuscript. The authors have no competing interests to declare.

CRediT authorship contribution statement

Bianca Schacherl: Conceptualization, Data curation, Formal analysis, Investigation, Methodology, Project administration, Validation, Visualization, Writing — original draft, Writing — review & editing. **Claudia Joseph:** Data curation, Investigation, Resources, Supervision, Writing — review & editing. **Polina Lavrova:** Investigation, Writing — review & editing. **Aaron Beck:** Investigation, Writing — review & editing. **Cédric Reitz:** Data curation, Writing — review & editing. **Tim Prüssmann:** Data curation, Methodology, Software, Writing — review & editing. **David Fellhauer:** Resources, Writing — review & editing. **Jun-Yeop Lee:** Investigation, Writing — review & editing. **Kathy Dardenne:** Resources, Writing — review & editing. **Jörg Rothe:** Methodology, Resources, Writing — review & editing. **Horst Geckeis:** Conceptualization, Funding acquisition, Resources, Writing — review & editing. **Tonya Vitova:** Conceptualization, Funding acquisition, Methodology, Project administration, Resources, Validation, Supervision, Writing — review & editing.

Declaration of competing interest

The authors declare that they have no known competing financial interests or personal relationships that could have appeared to influence the work reported in this paper.

Acknowledgements

The authors thank Kirsten Hardock and Alexander Gensch for the help with the design and technical drawing of the low

temperature cell and He environment. We acknowledge Volker Krepper and the INE workshop team for the construction of the low temperature cell and He environment. We thank the INE analytics group, especially Frank Geyer, for the ICP–MS analysis. We thank Jörg Göttlicher for the discussion on beam-induced changes, Enrique R. Batista for the discussion on statistical XANES analysis and Thomas Neill for his comments, which helped to improve the manuscript. We thank the Institute for Beam Physics and Technology (IBPT) for the operation of the storage ring, the Karlsruhe Research Accelerator (KARA).

Appendix A. Supplementary data

Supplementary data to this article can be found online at https://doi.org/10.1016/j.aca.2022.339636.

References

[1] H. Geckeis, J. Lützenkirchen, R. Polly, T. Rabung, M. Schmidt, Mineral−water interface reactions of actinides, Chem. Rev. 113 (2013) 1016−1062, https://doi.org/10.1021/cr300370h.
[2] Arbeitskreis Auswahlverfahren Endlagerstandorte (Akend), Auswahlverfahren für Endlagerstandorte, W&S Druck GmbH, Köln, 2002.
[3] Committee on Radioactive Waste Management (CoRWM), Managing Our Radioactive Waste Savely, CoRWM Doc 700, London, 2006.
[4] National Cooperative for the Disposal of Radioactive Waste (Nagra), Project Opalinus Clay: Safety Report - Demonstration of disposal feasibility for spent fuel, vitrified high-level wasteand long-lived intermediate-level waste (Entsorgungsnachweis), Nagra, Wettingen, 2002. Technical Report 02-05.
[5] National Cooperative for the Disposal of Radioactive Waste (Nagra), Projekt Opalinuston: Synthese der geowissenschaftlichen Untersuchungsergebnisse - Entsorgungsnachweis für abgebrannte Brennelemente, verglaste hochaktive sowie langlebige mittelaktive Abfälle, Nagra, Wettingen, 2002. Technical Report 02-03.
[6] E. Zeelmaekers, M. Honty, A. Derkowski, J. Środoń, M. De Craen, N. Vandenberghe, R. Adriaens, K. Ufer, L. Wouters, Qualitative and quantitative mineralogical composition of the rupelian Boom clay in Belgium, Clay Miner. 50 (2015) 249−272, https://doi.org/10.1180/claymin.2015.050.2.08.
[7] F. Claret, A. Bauer, T. Schäfer, L. Griffault, B. Lanson, Experimental investigation of the interaction of clays with high-pH solutions: a case study from the Callovo-Oxfordian formation, Meuse-Haute Marne underground laboratory (France), Clay Clay Miner. 50 (2002) 633−646, https://doi.org/10.1346/000986002320679369.
[8] D.R. Fröhlich, Sorption of neptunium on clays and clay minerals − a review, Clay Clay Miner. 63 (2015) 262−276, https://doi.org/10.1346/CCMN.2015.0630402.
[9] R. Marsac, N.L. Banik, J. Lützenkirchen, C.M. Marquardt, K. Dardenne, D. Schild, J. Rothe, A. Diascorn, T. Kupcik, T. Schäfer, H. Geckeis, Neptunium redox speciation at the illite surface, Geochem. Cosmochim. Acta 152 (2015) 39−51, https://doi.org/10.1016/j.gca.2014.12.021.
[10] N.L. Banik, R. Marsac, J. Lützenkirchen, C.M. Marquardt, K. Dardenne, J. Rothe, K. Bender, H. Geckeis, Neptunium sorption and redox speciation at the illite surface under highly saline conditions, Geochem. Cosmochim. Acta 215 (2017) 421−431, https://doi.org/10.1016/j.gca.2017.08.008.
[11] M.R. Antonio, L. Soderholm, X-ray absorption spectroscopy of the actinides in: the chemistry of the actinide and transactinide elements, Springer Netherlands, Dordrecht, 2006, https://doi.org/10.1007/1-4020-3598-5_28.
[12] M.A. Denecke, Actinide speciation using X-ray absorption fine structure spectroscopy, Coord. Chem. Rev. 250 (2006) 730−754, https://doi.org/10.1016/j.ccr.2005.09.004.
[13] L. Soderholm, M.R. Antonio, C. Williams, S.R. Wasserman, XANES spectroelectrochemistry: a new method for determining formal potentials, Anal. Chem. 71 (1999) 4622−4628, https://doi.org/10.1021/ac990080t.
[14] S.D. Conradson, D.L. Clark, M.P. Neu, W.H. Runde, C.D. Tait, Characterizing the plutonium aquo ions by XAFS spectroscopy, Los Alamos Sci. 26 (2000) 418−421.
[15] D.L. Clark, The chemical complexities of plutonium, Los Alamos Sci. 26 (2000) 364−381.
[16] P.S. Bagus, B. Schacherl, T. Vitova, Computational and spectroscopic tools for the detection of bond covalency in Pu(IV) materials, Inorg. Chem. 60 (21) (2021) 16090−16102, https://doi.org/10.1021/acs.inorgchem.1c01331.
[17] R. Polly, B. Schacherl, J. Rothe, T. Vitova, Relativistic multiconfigurational Ab initio calculation of uranyl 3d4f resonant inelastic X-ray scattering, Inorg. Chem. 60 (2021) 18764−18776, https://doi.org/10.1021/acs.inorgchem.1c02364.
[18] T. Vitova, I. Pidchenko, D. Fellhauer, P.S. Bagus, Y. Joly, T. Prüßmann, S. Bahl, E. Gonzalez-Robles, J. Rothe, M. Altmaier, M.A. Denecke, H. Geckeis, The role of the 5f valence orbitals of early actinides in chemical bonding, Nat. Commun. 8 (2017) 16053, https://doi.org/10.1038/ncomms16053.
[19] T. Vitova, M.A. Denecke, J. Göttlicher, K. Jorissen, J.J. Kas, K. Kvashnina, T. Prüßmann, J.J. Rehr, J. Rothe, Actinide and lanthanide speciation with high-energy resolution X-ray techniques, J. Phys. Conf. Ser. 430 (2013) 3−7, https://doi.org/10.1088/1742-6596/430/1/012117.
[20] I. Pidchenko, K.O. Kvashnina, T. Yokosawa, N. Finck, S. Bahl, D. Schild, R. Polly, E. Bohnert, A. Rossberg, J. Göttlicher, K. Dardenne, J. Rothe, T. Schäfer, H. Geckeis, T. Vitova, Uranium redox transformations after U(VI) coprecipitation with magnetite nanoparticles, Environ. Sci. Technol. 51 (2017) 2217−2225, https://doi.org/10.1021/acs.est.6b04035.
[21] T. Vitova, I. Pidchenko, D. Schild, T. Prüßmann, V. Montoya, D. Fellhauer, X. Gaona, E. Bohnert, J. Rothe, R.J. Baker, H. Geckeis, Competitive reaction of neptunium(V) and uranium(VI) in potassium−sodium carbonate-rich aqueous media: speciation study with a focus on high-resolution X-ray spectroscopy, Inorg. Chem. 59 (2020) 8−22, https://doi.org/10.1021/acs.inorgchem.9b02463.
[22] K.O. Kvashnina, S.M. Butorin, P. Martin, P. Glatzel, Chemical state of complex uranium oxides, Phys. Rev. Lett. 111 (2013) 1−5, https://doi.org/10.1103/PhysRevLett.111.253002.
[23] P. Glatzel, T.-C. Weng, K. Kvashnina, J. Swarbrick, M. Sikora, E. Gallo, N. Smolentsev, R.A. Mori, Reflections on hard X-ray photon-in/photon-out spectroscopy for electronic structure studies, J. Electron. Spectrosc. Relat. Phenom. 188 (2013) 17−25, https://doi.org/10.1016/j.elspec.2012.09.004.
[24] S. Bahl, S. Peuget, I. Pidchenko, T. Prüßmann, J. Rothe, K. Dardenne, J. Delrieu, D. Fellhauer, C. Jégou, H. Geckeis, T. Vitova, Pu coexists in three oxidation states in a borosilicate glass: implications for Pu solubility, Inorg. Chem. 56 (2017) 13982−13990, https://doi.org/10.1021/acs.inorgchem.7b02118.
[25] V. Häußler, S. Amayri, A. Beck, T. Platte, T.A. Stern, T. Vitova, T. Reich, Uptake of actinides by calcium silicate hydrate (C-S-H) phases, Appl. Geochem. 98 (2018) 426−434, https://doi.org/10.1016/j.apgeochem.2018.08.021.
[26] K.O. Kvashnina, A.Y. Romanchuk, I. Pidchenko, L. Amidani, E. Gerber, A. Trigub, A. Rossberg, S. Weiss, K. Popa, O. Walter, R. Caciuffo, A.C. Scheinost, S.M. Butorin, S.N. Kalmykov, A novel metastable pentavalent plutonium solid phase on the pathway from aqueous plutonium(VI) to PuO_2 nanoparticles, Angew. Chem. Int. Ed. 58 (2019) 17558−17562, https://doi.org/10.1002/anie.201911637.
[27] E. Gerber, A.Y. Romanchuk, I. Pidchenko, L. Amidani, A. Rossberg, C. Hennig, G.B.M. Vaughan, A. Trigub, T. Egorova, S. Bauters, T. Plakhova, M.O.J.Y. Hunault, S. Weiss, S.M. Butorin, A.C. Scheinost, S.N. Kalmykov, K.O. Kvashnina, The missing pieces of the PuO_2 nanoparticle puzzle, Nanoscale 12 (2020) 18039−18048, https://doi.org/10.1039/D0NR03767B.
[28] S. Kumar, J. Rothe, N. Finck, T. Vitova, K. Dardenne, A. Beck, D. Schild, H. Geckeis, Effect of manganese on the speciation of neptunium(V) on manganese doped magnetites, Colloids Surf. A Physicochem. Eng. Asp. 635 (2022) 128105, https://doi.org/10.1016/j.colsurfa.2021.128105.
[29] K. Müller, A. Gröschel, A. Rossberg, F. Bok, C. Franzen, V. Brendler, H. Foerstendorf, In situ spectroscopic identification of neptunium(V) inner-sphere complexes on the hematite-water interface, Environ. Sci. Technol. 49 (2015) 2560−2567, https://doi.org/10.1021/es5051925.
[30] C. Yang, B.A. Powell, S. Zhang, L. Rao, C. Yang, S. Zhang, L. Rao, Surface complexation modeling of neptunium(V) sorption to lepidocrocite (γ-FeOOH), Radiochim. Acta 103 (2015) 707−717, https://doi.org/10.1515/ract-2015-2405.
[31] A.C. Scheinost, R. Steudtner, R. Hübner, S. Weiss, F. Bok, Neptunium(V) retention by siderite under anoxic conditions: precipitation of NpO_2-like nanoparticles and of Np(IV) pentacarbonate, Environ. Sci. Technol. 50 (2016) 10413−10420, https://doi.org/10.1021/acs.est.6b02399.
[32] J.M. Combes, C.J. Chisholm-Brause, G.E. Brown, G.A. Parks, S.D. Conradson, P.G. Eller, I.R. Triay, D.E. Hobart, A. Miejer, EXAFS spectroscopic study of neptunium(V) sorption at the α-FeOOH/water interface, Environ. Sci. Technol. 26 (1992) 376−382, https://doi.org/10.1021/es00026a020.
[33] P. Bots, S. Shaw, G.T.W. Law, T.A. Marshall, J.F.W. Mosselmans, K. Morris, Controls on the fate and speciation of Np(V) during iron (oxyhydr)oxide crystallization, Environ. Sci. Technol. 50 (2016) 3382−3390, https://doi.org/10.1021/acs.est.5b05571.
[34] Y. Arai, P.B. Moran, B.D. Honeyman, J.A. Davis, In situ spectroscopic evidence for neptunium(V)-carbonate inner-sphere and outer-sphere ternary surface complexes on hematite surfaces, Environ. Sci. Technol. 41 (2007) 3940−3944, https://doi.org/10.1021/es062468t.
[35] X. Gaona, R. Dähn, J. Tits, A.C. Scheinost, E. Wieland, Uptake of Np(IV) by C-S-H phases and cement paste: an EXAFS study, Environ. Sci. Technol. 45 (2011) 8765−8771, https://doi.org/10.1021/es2012897.
[36] X. Gaona, E. Wieland, J. Tits, A.C. Scheinost, R. Dähn, Np(V/VI) redox chemistry in cementitious systems: XAFS investigations on the speciation under anoxic and oxidizing conditions, Appl. Geochem. 28 (2013) 109−118, https://doi.org/10.1016/j.apgeochem.2012.10.024.
[37] D.A. Dzombak, F.M.M. Morel, Surface complexation modeling: Hydrous ferric oxide, Wiley Interscience, New York, 1990.
[38] O. Elo, K. Müller, A. Ikeda-Ohno, F. Bok, A.C. Scheinost, P. Hölttä, N. Huittinen, Batch sorption and spectroscopic speciation studies of neptunium uptake by montmorillonite and corundum, Geochem. Cosmochim. Acta 198 (2017) 168−181, https://doi.org/10.1016/j.gca.2016.10.040.
[39] S. Virtanen, F. Bok, A. Ikeda-Ohno, A. Rossberg, J. Lützenkirchen, T. Rabung, J. Lehto, N. Huittinen, The specific sorption of Np(V) on the corundum (α-Al_2O_3) surface in the presence of trivalent lanthanides Eu(III) and Gd(III): a batch sorption and XAS study, J. Colloid Interface Sci. 483 (2016) 334−342,

https://doi.org/10.1016/j.jcis.2016.08.035.
[40] S.N. Kalmykov, V.V. Kriventsov, Y.A. Teterin, A.P. Novikov, Plutonium and neptunium speciation bound to hydrous ferric oxide colloids, Compt. Rendus Chem. 10 (2007) 1060–1066, https://doi.org/10.1016/j.crci.2007.06.015.
[41] M.A. Denecke, Synchrotron applications to f-element research in the nuclear fuel cycle, Dalton Trans. 44 (2015) 2606–2612, https://doi.org/10.1039/c4dt02716g.
[42] R. Terzano, M.A. Denecke, G. Falkenberg, B. Miller, D. Paterson, K. Janssens, Recent advances in analysis of trace elements in environmental samples by X-ray based techniques (IUPAC Technical Report), Pure Appl. Chem. 91 (2019) 1029–1063, https://doi.org/10.1515/pac-2018-0605.
[43] T. Reich, S. Amayri, P.J.B. Börner, J. Drebert, D.R. Fröhlich, D. Grolimund, U. Kaplan, Speciation of neptunium during sorption and diffusion in natural clay, J. Phys. Conf. Ser. 712 (2016) 1–4, https://doi.org/10.1088/1742-6596/712/1/012081.
[44] A.C. Scheinost, J. Claussner, J. Exner, M. Feig, S. Findeisen, C. Hennig, K.O. Kvashnina, D. Naudet, D. Prieur, A. Rossberg, M. Schmidt, C. Qiu, P. Colomp, C. Cohen, E. Dettona, V. Dyadkin, T. Stumpf, ROBL-II at ESRF: a synchrotron toolbox for actinide research, J. Synchrotron Radiat. 28 (2021) 333–349, https://doi.org/10.1107/S1600577520014265.
[45] W. Matz, N. Schell, G. Bernhard, F. Prokert, T. Reich, J. Claußner, W. Oehme, R. Schlenk, S. Dienel, H. Funke, F. Eichhorn, M. Betzl, D. Pröhl, U. Strauch, G. Hüttig, H. Krug, W. Neumann, V. Brendler, P. Reichel, M.A. Denecke, H. Nitsche, ROBL - a CRG beamline for radiochemistry and materials research at the ESRF, J. Synchrotron Radiat. 6 (1999) 1076–1085, https://doi.org/10.1107/S0909049599010663.
[46] K.F. Smith, N.D. Bryan, G.T.W. Law, R. Hibberd, S. Shaw, F.R. Livens, S.A. Parry, J.F.W. Mosselmans, K. Morris, Np(V) sorption and solubility in high pH calcite systems, Chem. Geol. 493 (2018) 396–404, https://doi.org/10.1016/j.chemgeo.2018.06.016.
[47] K. Gückel, A. Rossberg, K. Müller, V. Brendler, G. Bernhard, H. Foerstendorf, Spectroscopic identification of binary and ternary surface complexes of Np(V) on gibbsite, Environ. Sci. Technol. 47 (2013) 14418–14425, https://doi.org/10.1021/es4034183.
[48] D.R. Fröhlich, S. Amayri, J. Drebert, D. Grolimund, J. Huth, U. Kaplan, J. Krause, T. Reich, Speciation of Np(V) uptake by Opalinus Clay using synchrotron microbeam techniques, Anal. Bioanal. Chem. 404 (2012) 2151–2162, https://doi.org/10.1007/s00216-012-6290-2.
[49] F. Heberling, B. Brendebach, D. Bosbach, Neptunium(V) adsorption to calcite, J. Contam. Hydrol. 102 (2008) 246–252, https://doi.org/10.1016/j.jconhyd.2008.09.015.
[50] F. Heberling, A.C. Scheinost, D. Bosbach, Formation of a ternary neptunyl(V) biscarbonato inner-sphere sorption complex inhibits calcite growth rate, J. Contam. Hydrol. 124 (2011) 50–56, https://doi.org/10.1016/j.jconhyd.2011.02.002.
[51] H.E. Roberts, K. Morris, J.F.W. Mosselmans, G.T.W. Law, S. Shaw, Neptunium reactivity during co-precipitation and oxidation of Fe(II)/Fe(III) (oxyhydr)oxides, Geosci. 9 (2019), https://doi.org/10.3390/geosciences9010027.
[52] P.A. Wilk, D.A. Shaughnessy, R.E. Wilson, H. Nitsche, Interfacial interactions between Np(V) and manganese oxide minerals manganite and hausmannite, Environ. Sci. Technol. 39 (2005) 2608–2615, https://doi.org/10.1021/es040080x.
[53] M.A. Denecke, K. Dardenne, C.M. Marquardt, Np(IV)/Np(V) valence determinations from Np L_3 edge XANES/EXAFS, Talanta 65 (2005) 1008–1014, https://doi.org/10.1016/j.talanta.2004.08.034.
[54] M.M. van Schooneveld, S. DeBeer, A close look at dose: toward L-edge XAS spectral uniformity, dose quantification and prediction of metal ion photoreduction, J. Electron. Spectrosc. Relat. Phenom. 198 (2015) 31–56, https://doi.org/10.1016/j.elspec.2014.12.001.
[55] J. Göttlicher, R. Steininger, S. Mangold, T. Spangenberg, V. Veselska, E. Eiche, M. Schneider, T. Neumann, G. Penkert, P. Penkert, Application of X-ray absorption spectroscopy in earth and environmental sciences, in: 17th International Conference on X-Ray Absorption Fine Structure, 22–27 July 2018, Kraków, Poland, 2018.
[56] R. Steininger, J. Göttlicher, S. Mangold, V. Veselska, Irradiation effect studies on a Cr(VI) model system, in: 17th International Conference on X-Ray Absorption Fine Structure, 22–27 July 2018, Kraków, Poland, 2018.
[57] J. Göttlicher, A. Kotelnikov, N. Suk, A. Kovalski, T. Vitova, R. Steininger, Sulfur K X-ray absorption near edge structure spectroscopy on the photochrome sodalite variety hackmanite, Z. Kristallogr. 228 (2013) 157–171, https://doi.org/10.1524/zkri.2012.1587.
[58] B. Schacherl, T. Prüssmann, K. Dardenne, K. Hardock, V. Krepper, J. Rothe, T. Vitova, H. Geckeis, Implementation of cryogenic tender X-ray HR-XANES spectroscopy at the ACT station of the CAT-ACT beamline at the KIT Light Source, J. Synchrotron Radiat. 29 (2022) 80–88, https://doi.org/10.1107/S1600577521012650.
[59] V. Gabis, Etude mineralogique et geochimique de la serie sedimentaire oligocene du Velay, Bull. Liaison Soc. Fr. Mineral. Cristallogr. 86 (1963) 315–354.
[60] V. Montoya, B. Baeyens, M.A. Glaus, T. Kupcik, M. Marques Fernandes, L. Van Laer, C. Bruggeman, N. Maes, T. Schäfer, Sorption of Sr, Co and Zn on illite: batch experiments and modelling including Co in-diffusion measurements on compacted samples, Geochem. Cosmochim. Acta 223 (2018) 1–20, https://doi.org/10.1016/j.gca.2017.11.027.
[61] M.A. Glaus, M. Aertsens, C.A.J. Appelo, T. Kupcik, N. Maes, L. Van Laer, L.R. Van Loon, Cation diffusion in the electrical double layer enhances the mass transfer rates for Sr^{2+}, Co^{2+} and Zn^{2+} in compacted illite, Geochem. Cosmochim. Acta 165 (2015) 376–388, https://doi.org/10.1016/j.gca.2015.06.014.
[62] D. Fellhauer, J. Rothe, M. Altmaier, V. Neck, J. Runke, T. Wiss, T. Fanghänel, Np(V) solubility, speciation and solid phase formation in alkaline $CaCl_2$ solutions. Part I: experimental results, Radiochim. Acta 104 (2016) 355–379, https://doi.org/10.1515/ract-2015-2489.
[63] D.L. Parkhurst, C.A.J. Appelo, User's guide to PHREEQC (Version 2) : a computer program for speciation, batch-reaction, one-dimensional transport, and inverse geochemical calculations, USGS, Denver, CO, 1999, https://doi.org/10.3133/wri994259. Water Resources Investigation Report 99-4259.
[64] R. Guillaumont, T. Fanghänel, V. Neck, J. Fuger, D.A. Palmer, I. Grenthe, M.H. Rand, Update on the chemical thermodynamics of uranium, neptunium, plutonium, americium and technetium (OECD/NEA ed.), Elsevier, Amsterdam, 2003.
[65] A. Zimina, K. Dardenne, M.A. Denecke, D.E. Doronkin, E. Huttel, H. Lichtenberg, S. Mangold, T. Prüßmann, J. Rothe, T. Spangenberg, R. Steininger, T. Vitova, H. Geckeis, J.-D. Grunwaldt, CAT-ACT — a new highly versatile X-ray spectroscopy beamline for catalysis and radionuclide science at the KIT synchrotron light facility ANKA, Rev. Sci. Instrum. 88 (2017) 1–12, https://doi.org/10.1063/1.4999928.
[66] M.R. Antonio, L. Soderholm, C.W. Williams, J.-P.P. Blaudeau, B.E. Bursten, Neptunium redox speciation, Radiochim. Acta 89 (2001) 17–25, https://doi.org/10.1016/j.gca.2014.12.021.
[67] A. Ikeda-Ohno, C. Hennig, A. Rossberg, H. Funke, A.C. Scheinost, G. Bernhard, T. Yaita, Electrochemical and complexation behavior of neptunium in aqueous perchlorate and nitrate solutions, Inorg. Chem. 47 (2008) 8294–8305, https://doi.org/10.1021/ic8009095.
[68] X. Gaona, J. Tits, K. Dardenne, X. Liu, J. Rothe, M.A. Denecke, E. Wieland, M. Altmaier, Spectroscopic investigations of Np(V/VI) redox speciation in hyperalkaline TMA-(OH, Cl) solutions, Radiochim. Acta 100 (2012) 759–770, https://doi.org/10.1524/ract.2012.1948.
[69] B. Brendebach, N.L. Banik, C.M. Marquardt, J. Rothe, M. Denecke, H. Geckeis, X-ray absorption spectroscopic study of trivalent and tetravalent actinides in solution at varying pH values, Radiochim. Acta 97 (2009) 701–708, https://doi.org/10.1524/ract.2009.1674.
[70] T. Vitova, J.C. Green, R.G. Denning, M. Löble, K. Kvashnina, J.J. Kas, K. Jorissen, J.J. Rehr, T. Malcherek, M.A. Denecke, Polarization dependent high energy-resolution X-ray absorption study of dicesium uranyl tetrachloride, Inorg. Chem. 54 (2015) 174–182, https://doi.org/10.1021/ic5020016.
[71] T. Vitova, I. Pidchenko, S. Biswas, G. Beridze, P.W. Dunne, D. Schild, Z. Wang, P.M. Kowalski, R.J. Baker, Dehydration of the uranyl peroxide studtite, $[UO_2(\eta^2\text{-}O_2)(H_2O)_2]\cdot 2H_2O$, affords a drastic change in the electronic structure: a combined X-ray spectroscopic and theoretical analysis, Inorg. Chem. 57 (2018) 1735–1743, https://doi.org/10.1021/acs.inorgchem.7b02326.
[72] Y. Podkovyrina, I. Pidchenko, T. Prüßmann, S. Bahl, J. Göttlicher, A. Soldatov, T. Vitova, Probing covalency in the UO_3 polymorphs by U M_4 edge HR- XANES, J. Phys. Conf. Ser. 712 (2016) 1–4, https://doi.org/10.1088/1742-6596/712/1/012092.
[73] N. Stojanovic, Stanford Synchrotron Radiation Lightsource: Experimental Station 4-1, Last updated 20.02.2018. https://www-ssrl.slac.stanford.edu/content/beam-lines/bl4-1 (accessed January 14, 2021).